

# Topological Aspect and Quantum Magnetoresistance of $\beta$ -Ag<sub>2</sub>Te

Wei Zhang, Rui Yu, Wanxiang Feng, Yugui Yao, Hongming Weng, Xi Dai, Zhong Fang  
*Beijing National Laboratory for Condensed Matter Physics,  
 and Institute of Physics, Chinese Academy of Sciences, Beijing 100190, China;*  
 (Dated: October 14, 2018)

To explain the unusual non-saturating linear magnetoresistance observed in silver chalcogenides, the quantum scenario has been proposed based on the assumption of gapless linear energy spectrum. Here we show, by first principles calculations, that  $\beta$ -Ag<sub>2</sub>Te with distorted anti-fluorite structure is in fact a topological insulator with gapless Dirac-type surface states. The characteristic feature of this new binary topological insulator is the highly anisotropic Dirac cone, in contrast to known examples, such as Bi<sub>2</sub>Te<sub>3</sub> and Bi<sub>2</sub>Se<sub>3</sub>. The Fermi velocity varies an order of magnitude by rotating the crystal axis.

PACS numbers: 71.20.-b, 73.20.r, 73.43.Qt

Ag<sub>2</sub>Te, one of silver chalcogenides, is known as Hesseite mineral in nature. It was used as ionic conductor at high temperature  $\alpha$  phase, and it undergoes a phase transition below 417 K into the  $\beta$  phase, a narrow gap semiconductor, where the ion migration is frozen and the compound is non-magnetic. The gap of  $\beta$ -Ag<sub>2</sub>Te is in the range of several tens meV [1], the mobility of carriers is high and the effective mass is of the order of  $10^{-2}m_0$  ( $m_0$  is the free electron mass) [2]. Unusually large and non-saturating linear magnetoresistance (MR) were observed in  $\beta$ -Ag<sub>2+ $\delta$</sub> Te for the field range 10~55000 Oe and temperature range 4.5~300 K [3], in contrast to the conventional theory of metal with closed Fermi surface, from which the quadratic (low-field) and saturating (high-field) MR is expected. This leads to the proposal of quantum MR by Abrikosov [4], where only the lowest Landau level remains occupied. However, for a quadratic energy spectrum, the Landau level spacing (which depends on the field linearly) is about 0.1 K estimated for  $\beta$ -Ag<sub>2</sub>Te at 10 Oe), which is too small [4]. It is therefore necessary to assume the gapless linear energy spectrum [4], such that the field dependence of Landau level spacing follows the square root rule ( $\Delta E_n \propto \sqrt{B}$ ), similar to case of Graphene. The linear energy spectrum may come from the strong disorder as pursued by Abrikosov, however, we will show in this paper that  $\beta$ -Ag<sub>2</sub>Te is in fact a topological insulator with gapless linear Dirac-type surface states. This raises the possibility that the observed unusual MR may largely come from the surface/interface contributions.

Topological insulator (TI), characterized by the Z<sub>2</sub>-invariance and protected by the time-reversal symmetry, is a new state of quantum matter [5–9]. It is different with trivial insulator in the sense that its bulk is insulating, while its surface supports metallic Dirac fermions. Exotic quantum phenomena, such as Majorana fermion [10], magnetoelectric effect [11], and quantum anomalous Hall effect [12], are expected from TIs. It has been demonstrated that TI can be realized in 2D systems, such as HgTe/CdTe quantum well [13], or 3D

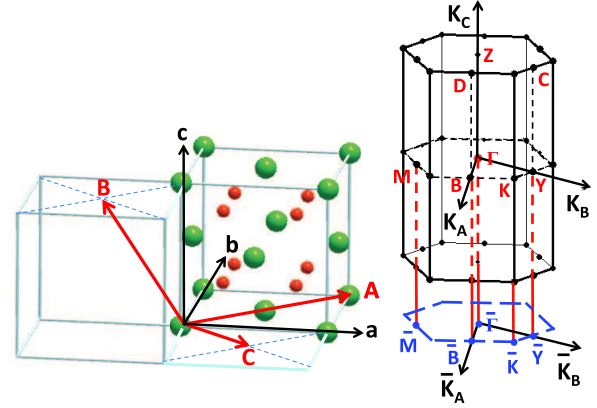


FIG. 1: (Color online) (a) The cubic anti-fluorite structure of  $\alpha$ -Ag<sub>2</sub>Te and its structural relationship to the  $\beta$  phase. The translational vectors of  $\alpha$  and  $\beta$  phases are labeled as  $a, b, c$  and  $A, B, C$ , respectively. (b) The Brillouin zone of  $\beta$ -Ag<sub>2</sub>Te, and its projected surface BZ to the plane perpendicular to  $C$ -axis.

materials like Bi<sub>1- $x$</sub> Sb <sub>$x$</sub>  [14]. The discovery of Bi<sub>2</sub>Se<sub>3</sub> family TIs with single Dirac cone on the surface is a significant progress [15], where the bulk gap is as large as 0.3 eV, which makes the room temperature applications possible. There are several more recent proposals, such as TlBiX<sub>2</sub> (X=Te, Se) compounds [16], ternary Heusler alloys [17], chalcopyrites [18], which all involve three or more elements, and may require additional distortions to open up the bulk gap. For all known TIs up to now, the surface Dirac cones are almost isotropic and Fermi velocity is nearly a constant. Here we will show that highly anisotropic surface Dirac cone can be obtained in  $\beta$ -Ag<sub>2</sub>Te, a new binary TI with distorted anti-fluorite structure.

We calculate the electronic structures of Ag<sub>2</sub>Te by using the WIEN2k package. The generalized gradient approximation (GGA) is used for the exchange-correlation functional, and Brillouin zone (BZ) is sampled with  $21 \times 21 \times 21$  grids for  $\alpha$  phase and  $10 \times 10 \times 10$  for  $\beta$  phase. We construct the projected atomic Wannier (PAW) func-

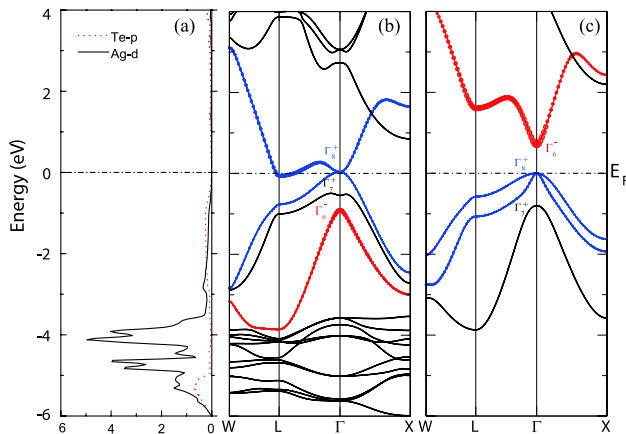


FIG. 2: (Color online) The calculated electronic structure of  $\alpha$ -Ag<sub>2</sub>Te. (a) The projected density of states. (b) The original band structure and (c) the one after pushing Ag-4d states artificially down to -20 eV. The projected component of Ag *s*-orbital is indicated as fat-bands.

tions [19] for *s* and *p* orbitals of Ag and Te. With this set of PAW bases, an effective model Hamiltonian for a slab of 45 layers along *C*-axis is established and the topologically nontrivial surface state is obtained from it.

The high temperature  $\alpha$ -phase of Ag<sub>2</sub>Te can be regarded as the anti-fluorite structure (shown in Fig. 1) in average [20]. Defining the cubic translational vectors as *a*, *b*, *c* ( $|a|=|b|=|c|$ ), this structure can be constructed from three fcc sub-lattices called as Te, Ag(1) and Ag(2) sub-lattice, respectively. The Ag(1) sub-lattice is shifted from the Te sub-lattice by a vector (*a*/4, *b*/4, *c*/4). If we only consider the Te and Ag(1) sub-lattices, it gives the same structure as zinc blende (like HgTe or CdTe). By adding the additional Ag(2) sub-lattice, which is shifted from original Te-fcc sub-lattice by ( $-a/4, -b/4, -c/4$ ), the anti-fluorite structure is obtained. Without distortions, the Ag(1) and Ag(2) sublattices are equivalent, and the space group is Fm3m with the inversion symmetry included. From the other point of view, if we divide the large cube defined by *a*, *b*, *c* into 8 small cubes, only 4 out of 8 cube's body centers are occupied in zinc blende, but they are now all occupied in anti-fluorite. All Ag atoms in  $\alpha$ -Ag<sub>2</sub>Te are tetrahedrally coordinated by four nearest neighboring Te atoms.

Fig. 2 shows the calculated band structure and density of states of  $\alpha$ -Ag<sub>2</sub>Te (with optimized lattice parameter  $a=6.8\text{\AA}$ ). The electronic structure can be well understood as zero-gap semiconductor, similar to HgTe, with inverted band ordering around the  $\Gamma$  point. In conventional zinc blende semiconductor, the anion-*p* states (Te-5*p*) at  $\Gamma$  point split into  $\Gamma_8$  and  $\Gamma_7$  manifolds due to the spin orbital coupling (SOC) with  $\Gamma_8$  forming the valence band maximum (VBM). The conduction band minimum (CBM) is mostly from the cation-*s* state, called as  $\Gamma_6$ . The  $\Gamma_6$  is typically higher than the  $\Gamma_8$  and  $\Gamma_7$ , such

as in CdTe, and a positive gap is formed. For HgTe, however, the situation is different due to the presence of Hg-5*d* states, which are very shallow and hybridize with Te-5*p* states strongly. Such hybridization will push the Te-5*p* upwards, resulting in an inverted band structure with the  $\Gamma_6$  state lower than the  $\Gamma_8$  (therefore a negative band gap). Due to the double degeneracy of  $\Gamma_8$  manifolds, the zero gap semiconductor is formed. The anti-fluorite structure of  $\alpha$ -Ag<sub>2</sub>Te is similar to zinc-blende, and its band structure is also very similar to HgTe. The Te sites form the same fcc sub-lattice with similar lattice parameters ( $a=6.8\text{\AA}$  for Ag<sub>2</sub>Te and  $a=6.46\text{\AA}$  for HgTe), but with two Ag atoms instead of single Hg atom in the unit cell. The low energy states of  $\alpha$ -Ag<sub>2</sub>Te can be also characterized as  $\Gamma_6, \Gamma_7, \Gamma_8$ . The Ag-4*d* level is again very shallow, located mostly from -6.0eV to -3.5eV as shown in Fig. 2. Since the Ag-4*d* orbitals are less extended than the Hg-5*d* orbitals, less *p-d* hybridization may be expected. However, because there are two Ag sites (instead of one Hg atom in HgTe) in one unit cell, the *p-d* hybridizations are strong enough to push up the Te-5*p* states and leads to the inverted band structure (as shown in Fig. 2(b)) with  $\Gamma_6$  lower than  $\Gamma_8$ . To further demonstrate this mechanism, we have shown in Fig. 2(c) the calculated band structure of  $\alpha$ -Ag<sub>2</sub>Te by artificially pushing the Ag-4*d* states down to -20 eV (out of the figure). Due to the reduced *p-d* hybridization, the Te-4*p* states are now lower than the Ag-5*s* states, giving a positive band gap.

The above calculations were done based on the GGA, which is known to underestimate the band gap of semiconductors (charge-transfer gap). The situation now is different with Bi<sub>2</sub>Te<sub>3</sub> and Bi<sub>2</sub>Se<sub>3</sub>, where the gap is formed within the *p* manifolds, and mostly due to the SOC, which is a local physics and can be well described by the GGA (or LDA) [15]. The band gap problem for HgTe and HgSe has been carefully studied by GW calculations and semi-empirical method [21], as well as comparing with experiments. It has been quantitatively suggested that the LDA underestimate the band gap of HgTe (or HgSe) by the magnitude around 0.3~0.6eV [21]. Considering the strong similarity between  $\alpha$ -Ag<sub>2</sub>Te and HgTe as discussed above, the same size of error bar from LDA (or GGA) may be expected. Nevertheless, even if the 0.6 eV correction for the band gap is added into our calculations, the resulting band structure still supports the inverted band ordering at  $\Gamma$ . This is because the calculated  $\Gamma_6$  in GGA is far below the  $\Gamma_8$  (about -1.0 eV), a number much bigger than the possible error bar for those compounds. Our results therefore suggest that Ag<sub>2</sub>Te has inverted band structure. This result is further confirmed by our calculations using hybrid functional [22]. As long as the inverted band ordering remains for Ag<sub>2</sub>Te, the topological nature can be expected as discussed for HgTe [13].

To turn a cubic zero-gap compound into a true semi-

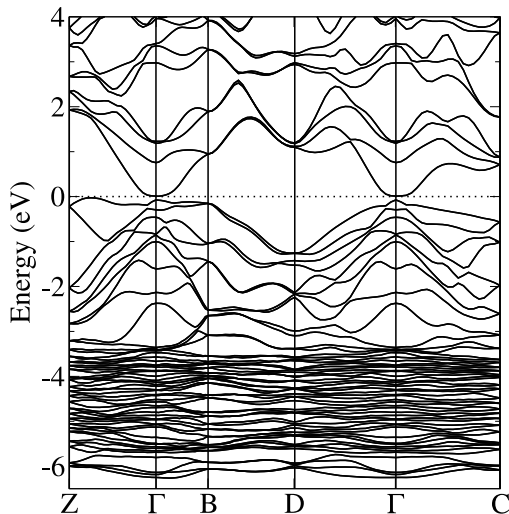


FIG. 3: (Color online) The calculated electronic structure of  $\beta$ -Ag<sub>2</sub>Te including spin-orbit coupling. A gap is opened around the Fermi level (indicated by the horizontal dotted line).

conductor with finite band gap, certain distortion or strain has to be introduced to break the symmetry and the degeneracy of  $\Gamma_8$  manifolds. This strategy has been followed for some of predicted topological insulators, such as Heusler alloys [17], although artificial distortions are not always easy. In our case, however, the Ag<sub>2</sub>Te undergoes structural distortion in its natural way: the high temperature  $\alpha$  phase changes into the  $\beta$  phase below 417 K, and the crystal structure of  $\beta$ -Ag<sub>2</sub>Te can be understood as the distorted anti-fluorite structure as shown in Fig. 1. Starting from the cubic  $\alpha$  phase with translational vectors  $a, b, c$ , we can define three new translational vectors  $A = a + b$ ,  $B = -a/2 - b/2 + c$ ,  $C = a/2 - b/2$ . Then the distortion happens in such a way that both the lengths of  $A, B, C$  vectors and the angle between the  $A$  and  $B$  axis are varied, while keeping the  $C$ -axis perpendicular to the  $AB$ -plane. The atomic positions are also shifted from their high-symmetrical position (of cubic phase), resulting in the monoclinic structure with space group  $P2_1/c$  [23]. Although the distortions are a bit complicated, the main effect of distortions in the electronic structure is to open up a gap around the Fermi level. Fig. 3 shows the calculated band structure of  $\beta$ -Ag<sub>2</sub>Te with SOC included (using experimental structure [23]). It is seen that the gap is around 80 meV, in good agreement with experimental data [1]. The present results can be also well compared to earlier calculations [24], except the fact that those studies neglected the SOC and therefore got metallic state.

The  $\beta$ -Ag<sub>2</sub>Te with distorted structure is now true insulating, but more importantly its topological nature is non-trivial due to the inverted band structure. Since the  $\beta$  phase has inversion symmetry, we can identify

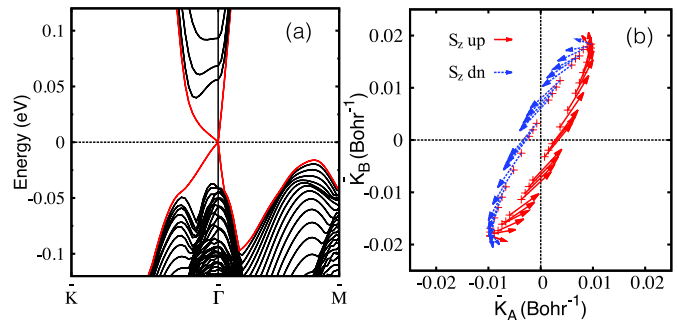


FIG. 4: (Color online) The surface states of  $\beta$ -Ag<sub>2</sub>Te for the surface perpendicular to  $C$ -axis. (a) The surface band structure and Dirac cone calculated from a slab of 45 layers; (b) The Fermi surface and spin texture of surface states with chemical potential located 10 meV below Dirac point. The in-plane components of spin are indicated as arrows, while the red (blue) color means the out of plane components pointing out-(in-) ward of the plane.

its topological nature by analyzing the parity of wave functions [9]. We have calculated the parities of occupied wave functions for time-reversal-invariant points in the BZ, it is confirmed that the product of parities of occupied bands is negative at  $\Gamma$  point and positive for other points, which leads to a  $Z_2=1$  topological insulator [9]. This topological nature should support gapless Dirac type surface states. The calculated surface state for the plane perpendicular to the  $C$ -axis is shown in the Fig. 4. It is clearly seen that we have single Dirac cone on the surface similar to Bi<sub>2</sub>Te<sub>3</sub>, and Bi<sub>2</sub>Se<sub>3</sub> [15, 19]. However, what is different is that the surface Dirac cone is highly anisotropic, and the Fermi velocity varies by about an order of magnitude moving around the cone. The broken rotational symmetry in this case is due to the absence of 4-fold (in HgTe) or 3-fold (in Bi<sub>2</sub>Se<sub>3</sub>) rotational symmetry. The spin direction is locked with lattice momentum and the spin chiral texture shown in Fig. 4 (b) corresponds to the chemical potential about 10 meV below the Dirac point. The spin direction of the surface states has out-of-plane component, which gives us more freedom to manipulate electron spin.

An effective  $k \cdot p$  model can be established by considering only the preserved time reversal symmetry for the surface state. The possible model Hamiltonian around  $\Gamma$  point is,

$$H(k) = A\sigma_x + B\sigma_y + C\sigma_z + DI_{2 \times 2}. \quad (1)$$

where  $\sigma_x, \sigma_y, \sigma_z$  are Pauli matrix and  $I_{2 \times 2}$  is  $2 \times 2$  identity matrix.  $A(k_x, k_y), B(k_x, k_y), C(k_x, k_y)$ , and  $D(k_x, k_y)$  are functions of lattice momentum. Here it is noticed that we have defined the principal axis  $z$  to be along the  $C$ -axis. In order to conserve the time reversal symmetry,  $A, B$  and  $C$  should contain only the odd terms of  $k_x$  and  $k_y$ , and  $D$  contains the even terms. We expand  $A$  and  $B$  up to the third order,  $D$  up to the second order,

while include only the linear term for  $C$  because the out-of-plane component of spin is much smaller than the in-plane component,

$$A(\vec{k}) = c_1 k_x + c_2 k_y + c_3 k_x^3 + c_4 k_x^2 k_y + c_5 k_x k_y^2 + c_6 k_y^3 \quad (2)$$

$$B(\vec{k}) = c_7 k_x + c_8 k_y + c_9 k_x^3 + c_{10} k_x^2 k_y + c_{11} k_x k_y^2 + c_{12} k_y^3 \quad (3)$$

$$C(\vec{k}) = c_{13} k_x + c_{14} k_y \quad (4)$$

$$D(\vec{k}) = c_{15} k_x^2 + c_{16} k_y^2 + c_{17} k_x k_y. \quad (5)$$

The parameters can be obtained by fitting the surface states calculated from *ab-initio*. Both the shape and spin orientation of surface states can be well reproduced with the parameters listed in Ref.[25].

The existence of gapless Dirac surface states in  $\beta$ -Ag<sub>2</sub>Te suggests that the observed unusual MR may have large contribution coming from the surface or interface. Due to the large Landau level spacing and high mobility, it can be estimated for  $\beta$ -Ag<sub>2</sub>Te that the quantum limit can be reached at about 10 K under only 10 Oe field, in good agreement with experiment [3]. Our scenario is further supported by the fact that experimental samples, doped with excess Ag, are granular materials [3, 26], which makes the surface/interface contribution significant. On the other hand, the highly anisotropic surface states may cause large fluctuation of mobility, which may also help to explain the unusual MR behavior [26]. We have done similar calculations for Ag<sub>2</sub>Se, and found that it is also topologically non-trivial with inverted band structure, while its  $\beta$  phase crystal structure is different with Ag<sub>2</sub>Te.

In summary, we have shown by first principles calculations that  $\beta$ -Ag<sub>2</sub>Te is a new binary topological insulator provided by nature, with highly anisotropic single surface Dirac cone. We suggest that the observed unusual MR behavior can be understood from its topological nature. We acknowledge the supports from NSF of China and that from the 973 program of China (No.2007CB925000).

---

[1] R. Dalven, Phys. Rev. Lett. **8**, 311 (1966); R. Dalven and R. Gill, Phys. Rev. **159**, 645 (1967); P. Junod, H. Hediger, B. Kilchör, and J. Wulschleger, Philos. Mag. **36**, 941 (1977).  
 [2] S. A. Aliev, and F. F. Aliev, Izv. Akad. Nauk SSSR, Neorg. Mater. **21**, 1869 (1985).  
 [3] R. Xu, A. Hussman, T. F. Rosenbaum, M.-L. Saboungi, J. E. Enderby, P. B. Littlewood, Nature **390**, 57 (1997).  
 [4] A. A. Abrikosov, Phys. Rev. B **58**, 2788 (1998).  
 [5] C. L. Kane, E. J. Mele, Phys. Rev. Lett. **95**, 146802 (2005).

[6] B. A. Bernevig, S. C. Zhang, Phys. Rev. Lett. **96**, 106802 (2006).  
 [7] J. E. Moore and L. Balents, Phys. Rev. B **75**, 121306 (2007).  
 [8] L. Fu, C. L. Kane, and E. J. Mele, Phys. Rev. Lett. **98**, 106803 (2007).  
 [9] L. Fu and C. L. Kane, Phys. Rev. B **76**, 045302 (2007).  
 [10] L. Fu, C. L. Kane, Phys. Rev. Lett. **100**, 096407 (2008); X.-L. Qi, T. L. Hughes, S. Raghu, S. C. Zhang, Phys. Rev. Lett., **102**, 187001 (2009).  
 [11] X.-L. Qi, T. L. Hughes, S.-C. Zhang, Phys. Rev. B **78**, 195424 (2008); A. M. Essin, J. E. Moore, and D. Vanderbilt, Phys. Rev. Lett. **102**, 146805 (2009).  
 [12] X. L. Qi, Y. S. Wu, S. C. Zhang, Phys. Rev. B **74**, 085308 (2006). F. D. M. Haldane, Phys. Rev. Lett. **61**, 2015 (1988). M. Onoda, N. Nagaosa, Phys. Rev. Lett. **90**, 206601 (2003); R. Yu, W. Zhang, H.-J. Zhang, S.-C. Zhang, X. Dai, Z. Fang, Science. **329**, 61 (2010).  
 [13] B. A. Bernevig, T. L. Hughes, S. C. Zhang, Science **314**, 1757 (2006); M. König, S. Wiedmann, C. Brüne, A. Roth, H. Buhmann, L. W. Molenkamp, X. L. Qi, and S. C. Zhang, Science **318**, 766 (2007); X. Dai, T. L. Hughes, X.-L. Qi, Z. Fang, S.-C. Zhang, Phys. Rev. B **77**, 125319 (2008).  
 [14] D. Hsieh, D. Qian, L. Wray, Y. Xia, Y. S. Hor, R. J. Cava, M. Z. Hasan, Nature **452**, 970 (2008); J. C. Y. Teo, L. Fu, C. L. Kane, Phys. Rev. B **78**, 045426 (2008); H.-J. Zhang, C.-X. Liu, X.-L. Qi, X.-Y. Deng, X. Dai, S.-C. Zhang, Z. Fang, Phys. Rev. B **80**, 085307 (2009).  
 [15] H. Zhang, C. X. Liu, X. L. Qi, X. Dai, Z. Fang, S.-C. Zhang, Nature Phys. **5**, 438 (2009); Y. Xia, et.al., Nature Phys. **5**, 398 (2009); Y. L. Chen, et.al., Science **325**, 178 (2009).  
 [16] B. Yan, C.-X. Liu, H.-J. Zhang, C.-Y. Yam, X.-L. Qi, T. Frauenheim, and S.-C. Zhang, Europhysics Letters **90**, 37002 (2010); T. Sato, K. Segawa, H. Guo, K. Sugawara, S. Souma, T. Takahashi, Y. Ando, W. Cai, D. Chen, Y. Ren, et al., Phys. Rev. Lett. **105**, 136802 (2010).  
 [17] H. Lin, L. A. Wray, Y. Xia, S. Xu, S. Jia, R. J. Cava, A. Bansil, and M. Z. Hasan, Nature Mater. **9**, 546 (2010); S. Chadov, X. L. Qi, and et.al., Nature Mater. **9**, 541 (2010); D. Xiao, Y. G. Yao, W. X. Feng, and et.al., Phys. Rev. Lett. **105**, 096404 (2010).  
 [18] W. Feng, J. Ding, D. Xiao, and Y. Yao, arXiv:1008.0056 (2010).  
 [19] W. Zhang, R. Yu, H. Zhang, X. Dai, Z. Fang, New J. Phys. **12**, 065013 (2010).  
 [20] H. Kikuchi, H. Iyetomi, A. Hasegawa, J. Phys.: Cond. Matt. **9**, 6031 (1997).  
 [21] C. Y. Moon, and S. H. Wei, Phys. Rev. B **74**, 045205 (2006); A. Fleszar, W. Hanke, Phys. Rev. B **71**, 045207 (2005).  
 [22] J. Heyd, G. E. Scuseria, and M. Ernzerhof, J. Chem. Phys. **124**, 219906 (2006).  
 [23] A. van der Lee, J. L. de Boer, Acta Crystallogr. C **49**, 1444 (1993).  
 [24] S. Kashida, N. Watanabe, T. Hasegawa, H. Iida, M. Mori, Solid State Ionics, **148**, 193 (2002); C. M. Fang, R. A. de Groot, G. A. Wieggers, J. Phys. Chem. Solids, **63**, 457 (2002).  
 [25] The fitted parameters (with energy unit in eV and length unit in Å) are:  $c_1=-1.192$ ,  $c_2=0.781$ ,  $c_3=-14.935$ ,  $c_4=17.443$ ,  $c_5=9.963$ ,  $c_6=11.609$ ,  $c_7=-1.807$ ,  $c_8=0.822$ ,  $c_9=-12.415$ ,  $c_{10}=13.148$ ,  $c_{11}=-55.148$ ,  $c_{12}=19.788$ ,  $c_{13}=-$

0.217,  $c_{14}=0.116$ ,  $c_{15}=-1.559$ ,  $c_{16}=2.687$ ,  $c_{17}=-9.705$ .

[26] M. M. Parish, P. B. Littlewood, *Nature*, **426**, 162 (2003).